Investigating the dynamics of droplet breakup in a microfluidic cross-slot device for characterizing the extensional properties of weakly-viscoelastic fluids

Kristin A. Marshall & Travis W. Walker

Rheologica Acta

ISSN 0035-4511

Rheol Acta
DOI 10.1007/s00397-019-01152-0

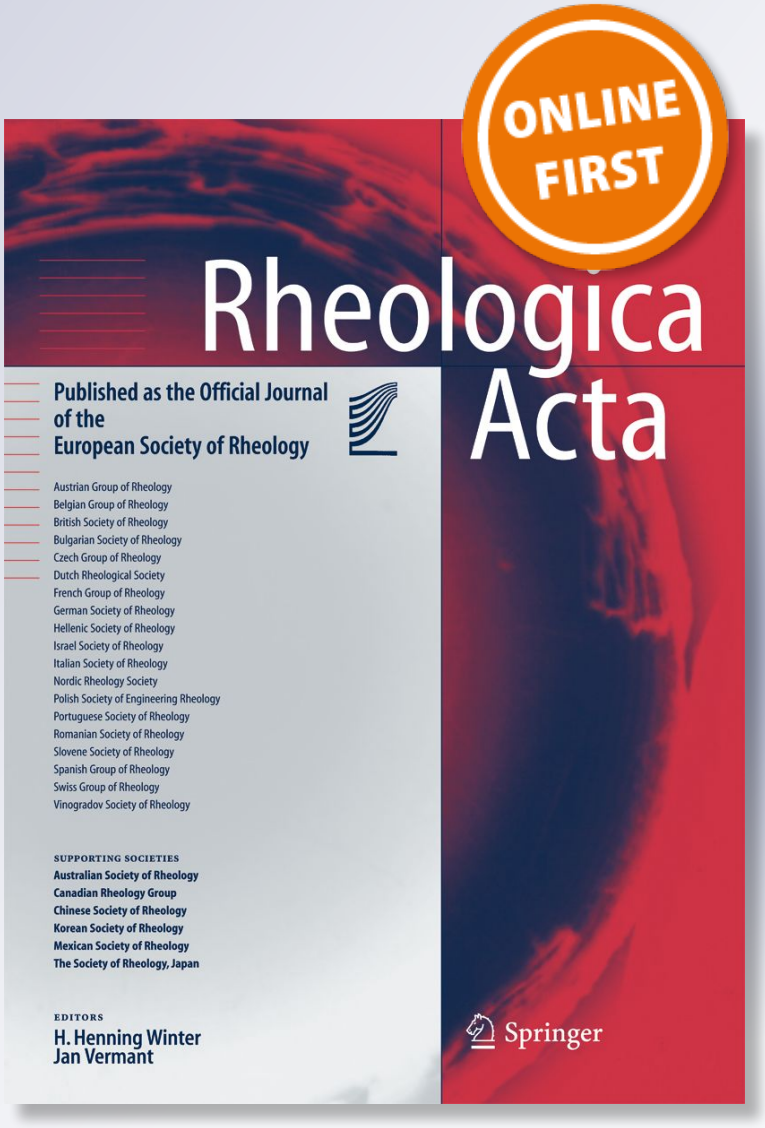

Springer

Rheologica Acta
https://doi.org/10.1007/s00397-019-01152-0

ORIGINAL CONTRIBUTION

Investigating the dynamics of droplet breakup in a microfluidic cross-slot device for characterizing the extensional properties of weakly-viscoelastic fluids

Kristin A. Marshall[1] · **Travis W. Walker**[2]

Received: 7 September 2018 / Revised: 28 April 2019 / Accepted: 1 May 2019

Abstract

A microfluidic device, deemed the Plateau-Rayleigh microfluidic extensional rheometer (PRIMER), is presented that uses a cross-slot geometry to observe a two-phase droplet-breakup event in which the viscoelastic fluid is in the dispersed (or droplet) phase. For viscoelastic fluids, we report that a cylindrical filament forms between droplet segments with a diameter that decays exponentially in time. In optically tracking this decay, both transient extensional viscosity and extensional relaxation times can be evaluated. For validating and optimizing the device, a range of poly(ethylene oxide) (PEO) solutions and Newtonian solutions were tested. Comparisons of the evolution profiles as a result of the presence of elasticity are made, and these results are compared with the results from dripping-onto-a-substrate (DoS), another emerging extensional technique.

Keywords Breakup · Viscoelasticity · Extensional flow · Drop deformation

Introduction

The addition of linear macromolecules to a solvent, even in dilute quantities, can significantly alter the response of a fluid to an extensional, or stretching, flow. When high-molecular-weight molecules are extended in solution, extensional thickening can result when polymer chains undergo coil-stretch transitions, producing extensional viscosities that can be orders of magnitude larger than values of viscosity that are found in shear flow. Such behavior is often manifested as the "stringy" or "tacky" nature of a fluid, and it will vary depending on the concentration, molecular weight, and type of the polymer that has been added to a given system. For dilute and semi-dilute polymer solutions, the presence of elasticity may not be apparent in steady or oscillatory shear flows, yet it may alter the response of a fluid when undergoing an extensional deformation. For example, during the process of inkjet printing, small amounts of polymer can be added to the ink to prevent unwanted satellite drops from diminishing the quality of the print (de Gans et al. 2004; Xu et al. 2007; Tuladhar and Mackley 2008; Morrison and Harlen 2010; Hoath et al. 2015). The presence of too much polymer, however, may lead to the failed ejection of the ink. Nevertheless, when performing shear rheometry, such inks may "appear" Newtonian, having zero-shear viscosities on the same order of magnitude as water, making predictions for the performance of the inks difficult to determine.

Other applications that employ small quantities of polymers include additives in subsurface flows (Jones and Walters 1989; Wever et al. 2011; Zhong et al. 2013), in turbulent drag reduction (Savins 1964; Paterson and Abernathy 1970; Virk 1975; Gyr and Bewersdorff 2013), and in enhanced particle removal (Walker et al. 2014). In each of these applications, the predominant mode of deformation is extensional, and the characteristic length scale is on the order of microns or less. Aside from the obvious need to measure the extensional properties of such dilute and semi-dilute polymer solutions, developing reliable characterization techniques has been a key focus in the field of rheology over the past 20 years (Petrie 2006).

✉ Travis W. Walker
travis.walker@sdsmt.edu

[1] School of Chemical, Biological, and Environmental Engineering, Oregon State University, Corvallis, OR, 97331, USA

[2] Department of Chemical and Biological Engineering, South Dakota School of Mines and Technology, Rapid City, SD, 57701, USA

Published online: 21 June 2019

Despite the numerous techniques that have been and continue to be developed, discrepancies resulting from pre-deformation history, an inability to provide a completely shear-free flow, and the transient nature of the growth of extensional stresses have led to inconsistencies in the measurements of the apparent extensional viscosity (Nguyen et al. 1990; Anna et al. 2001). Nevertheless, progress in the theoretical understanding of the behavior of extensional flows has inspired a new wave of experimental design (Entov and Hinch 1997; Wagner et al. 2005). As a result, a number of extensional techniques have been proposed that are capable of characterizing a range of materials from low-viscosity mobile polymer solutions (Fuller et al. 1987; Rodd et al. 2005; Sousa et al. 2017) to more viscous polymer melts (Cogswell 1972; James and Walters 1993; Collier et al. 1998; McKinley and Sridhar 2002) and that address problems such as solvent evaporation (Sousa et al. 2017). Of the techniques that are commercially available, the majority are suitable for more viscous fluids (McKinley and Sridhar 2002). Methods for characterizing low-viscosity and weakly-elastic fluids, on the other hand, are limited in number, and extending the range of testable materials continues to serve as an active area of research in the field (Arratia et al. 2008, 2009; Galindo-Rosales et al. 2013; Sousa et al. 2017). Further, our motivation to characterize materials for turbulent drag reduction necessitates the use of an apparatus that can prevent the volatile solvent from evaporating during the test, as the effect of concentration can be quite pronounced. For example, drag-reduction effects may still be noted for dilute polymer solutions that have no "apparent" elasticity when using more conventional characterization techniques. Presenting an alternative means for characterizing such fluids is the focus of the present study.

Relevant dimensionless parameters

To date, the most common approaches for characterizing the extensional properties of dilute and semi-dilute polymer solutions involve the thinning and breakup of filaments of samples that are formed between two surfaces. In such "filament-stretching rheometers," samples may either be continuously stretched by an external forcing or allowed to break under the action of capillary forces. The underlying dynamics of such techniques involve the interplay between competing viscous, elastic, inertial, and capillary effects. For such free-surface flows, one may consider a set of dimensionless parameters that are clearly outlined by McKinley (2005a, 2005b).

In the analysis, a parameter space is presented that depends on three core dimensionless groups that describe the size of the capillary, inertial, and elastic effects relative to the viscous stresses for a given processing environment. These core parameters include the capillary number, a ratio of viscous forces to capillary forces,

$$Ca = \frac{\eta_0 u^*}{\sigma}; \tag{1}$$

the Reynolds number, a ratio of inertial forces to viscous forces,

$$Re = \frac{\rho u^* \ell^*}{\eta_0}; \tag{2}$$

and the Weissenberg number, a ratio of elastic forces to viscous forces,

$$Wi = \frac{\lambda_E u^*}{\ell^*}; \tag{3}$$

respectively. Here, u^* and ℓ^* are the characteristic velocity and length scales of interest, ρ is the density, η_0 is the zero-shear viscosity, σ is the interfacial tension, and λ_E is the characteristic extensional relaxation time of the fluid.

A free-surface flow process can be fully described if the three parameters $\{Ca, Re, Wi\}$ are known. Furthermore, using these parameters, other dependent dimensionless groups can be formulated to better describe the relevant time scales that define filament-thinning processes. The Ohnesorge number, for example, compares the time scales for the breakup of a viscous thread relative with the breakup of an inviscid and inertially dominated jet, and it can be simplified as follows

$$Oh^2 = \frac{\eta_0^2}{\rho \sigma \ell^*} = \frac{Ca}{Re}. \tag{4}$$

Thus, to label a fluid to be "low-viscosity," the viscous time scale should be less than the inertial time scale such that the Ohnesorge number is less than unity, $Oh < 1$. Additionally, an "intrinsic" Deborah number is found when comparing the elastic time scale for the stress relaxation of polymer with the characteristic process time, and it is defined as

$$De^2 = \lambda_E^2 \left(\frac{\sigma}{\rho \ell^{*3}} \right) = \frac{Wi^2}{Re\, Ca}. \tag{5}$$

This Deborah number is independent of flow properties such as velocity. For fluids having low elasticity, or a short stress-relaxation time, the intrinsic Deborah number is often less than one. A third dimensionless group, the Weber number (We), describes the importance of inertial forces to capillary forces, and it is defined as

$$We = \frac{\rho u^{*2} \ell^*}{\sigma} = Re\, Ca. \tag{6}$$

The Weber number describes whether the filament-thinning process is caused by an external forcing ($We \gg 1$) or if the process is "self-thinning" ($We \ll 1$) . The present work focuses on the latter, in which capillary forces induce a filament-thinning and breakup event. In such experiments,

when $De > 1$ and $Oh > 1$, inertial forces are negligible, elastic and/or viscous forces balance capillary forces, and measurements can be performed. Further, if $De < 1$, the technique is still operable if $Oh > 1$, and such a fluid is deemed a *weakly-elastic fluid*. Likewise, if $Oh < 1$, the technique is still operable if $De > 1$, and such a fluid is deemed a *low-viscosity elastic fluid* (Harrison and Boger 2000; Rodd et al. 2005).

To evaluate a given processing environment, the core parameters can be compared. For example, in bulk flows of viscoelastic fluids where capillary effects are negligible, the Reynolds and Weissenberg numbers would be compared to describe the relative importance of inertial and elastic stresses. The ratio of these two parameters forms the elasticity number such that

$$El \equiv \frac{Wi}{Re} = \frac{\eta_0 \lambda_E}{\rho \ell^{*2}}. \tag{7}$$

In general, when the elasticity number is much greater than unity ($El \gg 1$), such as during the extrusion of a polymer melt for 3D printing, significant elastic effects are observed.

To date, the filament stretching extensional rheometer (FiSER), which works by continually stretching a sample while imposing a constant stress or strain rate, is the most rigorously analyzed experiment for determining extensional rheology, as the device provides the purest extensional flow field (Anna et al. 2001; McKinley and Sridhar 2002). However, the lack of commercial availability of the FiSER combined with the requirement of relatively high zero-shear viscosities and exposure to the atmosphere air makes this tool impractical for characterizing all low-viscosity elastic fluids and provides opportunities for less fundamental devices to provide insight into the effect of high-molecular-weight polymers on dilute solutions.

Capillary breakup extensional rheometry

Of the commercially available filament stretching rheometers, the Capillary Breakup Extensional Rheometer $\left(\text{CaBER}^{\text{TM}}\right)$ is one of the most capable instruments for measuring viscoelastic fluids with low shear viscosities, $\eta_0 \in \left[10^1, 10^3\right]$, mPa·s. First presented experimentally by Bazilevsky et al. (1990) and developed theoretically by Entov and co-workers (Entov and Hinch 1997), capillary breakup extensional rheometry monitors the gradual necking and breakup of a self-thinning filament under the action of capillary forces. Unlike the FiSER, the CaBER applies a finite step-strain to a material that is initially loaded between two parallel plates, forming an unstable filament (Matta and Tytus 1990; McKinley and Sridhar 2002).

In-depth discussions on the early-, middle-, and late-time dynamics of the capillary-driven thinning and breakup processes of a cylindrical filament are provided in the literature (Entov and Hinch 1997; Mckinley 2005b). For quantifying the elastic properties of a sample, the filament-thinning dynamics of interest occur in the middle regime in which elastic stresses dominate over viscous stresses to counteract the capillary pressures that are driving the breakup event. For dilute and semi-dilute polymer solutions, the diameter of a cylindrical filament, D, has been shown to thin exponentially in time, independent of the position in the z-coordinate, according to

$$\frac{D(t)}{D_1} = \left[\frac{G D_1}{4\sigma}\right]^{1/3} \exp\left[-\frac{t}{3\lambda_E}\right], \tag{8}$$

such that D_1 is the diameter of the sample after the initial step-strain has been applied, and G is the shear relaxation modulus (Entov and Hinch 1997; Clasen et al. 2006a).

For the uniaxial extension of a cylindrical filament at a constant strain rate, the diameter of the filament will decay according to

$$D(t) = D_1 \exp\left[-\frac{\dot{\varepsilon} t}{2}\right], \tag{9}$$

such that $\dot{\varepsilon}$ is the extensional strain rate (Macosko 1994). Comparing Eqs. 8 and 9, the strain rate in the middle elastocapillary regime is found to be inversely proportional to the characteristic extensional relaxation time, independent of pre-strain and the initial aspect ratio of the filament. The corresponding Weissenberg number is a constant, $Wi = \lambda_E \dot{\varepsilon} = 2/3$, which is above a critical value, $Wi_{cr} = 1/2$, where individual polymer chains can be significantly strained from their equilibrium conformations to undergo coil-stretch transitions (De Gennes 1974; Hinch 1974). Thus, once a filament is formed, it thins at a strain rate that is established by the elastic properties of the fluid. Such thinning behavior has been investigated and observed over a range of polymer types, concentrations, and molecular weights (Liang and Mackley 1994; Anna and McKinley 2001; Clasen et al. 2004). By evaluating the force balance between viscous, elastic, and capillary stresses that are acting within a sample, the CaBER technique can be used to approximate the transient extensional viscosity $\left(\eta_E^+(\varepsilon)\right)$ as a function of Hencky strain, ε (Macosko 1994; Mckinley 2005b).

Several contributors have added to the CaBER technique, both experimentally and theoretically in predicting the evolution of self-thinning filaments for various constitutive models (Kolte and Szabo 1999; McKinley and Tripathi 2000; Clasen et al. 2004; Rodd et al. 2005; Dinic et al. 2015; Wagner et al. 2015; Sousa et al. 2017). Although Eq. 8 was developed for monodisperse solutions, the exponential relationship has held true for other polymeric solutions of varying concentrations and molecular weights that are investigated in the literature (Bazilevsky et al. 1990; Liang

and Mackley 1994; Anna and McKinley 2001; Anna et al. 2001; Clasen et al. 2004). In addition, multi-mode models have been developed, indicating that the presence of shorter relaxation times contribute to the initial rapid decay of the filament, whereas the longest relaxation time is responsible for the late-time decay that is exponential (Anna and McKinley 2001; Clasen et al. 2006b). At late times in the thinning process, as the filament necks and breaks, large extensional strains are achieved. Finite extensibility of the polymer chains allows for a filament to break in a finite amount of time (Renardy 1995; Entov and Hinch 1997), which can possibly obscure the exponential-thinning region (Clasen et al. 2006b).

The limits of operation for the CaBER have been summarized by Rodd and McKinley in an operability diagram (Rodd et al. 2005). Under optimal conditions, the minimum measurable relaxation time has been projected to be 1 ms for liquids with a shear viscosity of 3 mPa·s. A more appropriate description of CaBER limitations employs the dimensionless numbers that are described in "Relevant dimensionless parameters" that describe self-thinning filaments.

Additional limiting factors for the CaBER include gravitational sagging (Anna and McKinley 2008), the finite time that is required to impose an initial axial deformation (Miller et al. 2009), and concerns regarding endplate effects (Spiegelberg et al. 1996; Dinic et al. 2015; Dinic et al. 2017). Recent improvements extending the capabilities of the CaBER technique include the use of a high-speed camera that is combined with a slow-retraction method (SRM) to capture the rapid filament-thinning process (Campo-Deano and Clasen 2010).

Efforts to extend the range of the fluids that can be characterized are ongoing. At lower concentrations of polymer, a filament-breakup process transitions from being dominated by the characteristic time scale of the polymer to being dominated by the viscocapillary or inertiocapillary time scales (Mckinley 2005a). The elastocapillary number, Ec, is used to describe the relative elastic effects for a given system. The elastocapillary number compares the viscous and elastic time scales, and it is found to be the ratio of the intrinsic Deborah number to the Ohnesorge number

$$Ec = \frac{\lambda_E \sigma}{\eta_0 \ell^*} = \frac{De}{Oh} = \frac{Wi}{Ca}. \tag{10}$$

As this number becomes greater than unity, elastic effects are said to be more distinguishable relative to viscous effects (Mckinley 2005b; Clasen et al. 2006b; Galindo-Rosales et al. 2013). Since the elastocapillary number is proportional to the inverse of the characteristic length scale, the effects of elasticity become more pronounced as the size of the system is decreased. For these reasons, microfluidic devices are being considered for their potential to extend the range of fluids that can traditionally be characterized.

Microfluidic devices for extensional characterization

Microfluidic techniques provide opportunities for potentially characterizing low-viscosity and weakly-elastic fluids. The goal of the present work was to apply the capillary-breakup process, which has already been well defined on the macroscale (Stone et al. 1986; Stone and Leal 1989, 1990; Tjahjadi et al. 1992; Stone 1994; Lister and Stone 1998), to the microscale. A recent review discusses attempts that have been made to incorporate the small length scales of microfluidic devices for characterizing the extensional properties of low-viscosity and weakly-elastic fluids (Arratia et al. 2008, 2009; Christopher and Anna 2009; Galindo-Rosales et al. 2013; Sousa et al. 2017). Sousa et al. (Sousa et al. 2017), for example, have presented a micro-CaBER that is capable of measuring relaxation times that are below one millisecond with weakly-viscoelastic polymer solutions. Furthermore, the optimized cross-slot device (OSCER) that was developed by McKinley and co-workers has proven successful in providing constant, homogeneous extension rates at low Reynolds numbers, and it has already been used for characterizing fluids such as hyaluronic acid (Haward et al. 2012, 2014). A recent review of microfluidic extensional rheometry using flows at stagnation points was presented by Haward (2016). Although the cross-slot techniques that have been described monitor the behavior of a single-phase flow, two-phase droplet breakup at the center of a cross-slot geometry has yet to be investigated. Other microfluidic techniques of relevance include the microscopic adaptations of the four-roll mill (Hudson et al. 2004; Lee et al. 2007).

The present study investigates the use of droplet breakup in a cross-slot geometry for the extensional characterization of low-viscosity complex fluids, particularly for fluids that cannot be characterized using traditional capillary-breakup techniques. Although the passive breakup of droplets at a T-junction has been previously suggested as a means for characterizing low-viscosity and weakly-elastic fluids (Christopher and Anna 2009), the present study aimed to validate and expand on such ideas, adding a symmetry component to the droplet-splitting environment. In the present work, a Plateau-Rayleigh instability microfluidic extensional rheometer (PRIMER) is presented that uses a cross-slot geometry to initiate a droplet-breakup event at the stagnation point. For viscoelastic samples, filaments that form were evaluated using the same approach as filaments that form in CaBER experiments.

The present work compared the breakup dynamics of a range of polymer solutions and Newtonian solutions with comparable shear viscosities. Both the concentration of

polymer and the global parameters of the cross-slot device were investigated for their impact on the droplet-breakup event. In particular, we observed how flow rates and the selection of the outer viscous fluid impact measurement results. The early-, middle-, and late-time dynamics of the droplet-breakup process are monitored and compared for a variety of flow conditions and previous studies (Link et al. 2004; Husny and Cooper-White 2006; Garstecki et al. 2006; Xu et al. 2008; Christopher and Anna 2009). For the present text, only the diameter-decay profiles and the resulting characteristic extensional relaxation times are reported.

Methods and materials

Microfluidic design and fabrication

The PRIMER device that was developed for the present study consists of two main geometries including a T-junction that is used for droplet formation and a cross slot that is used to initiate a droplet-breakup event (Fig. 1). The generation of Newtonian and viscoelastic droplets at T-junction geometries is well described in the literature (Garstecki et al. 2006; Husny and Cooper-White 2006; Xu et al. 2006; De Menech et al. 2008; van Steijn et al. 2010).

In general, a cross-slot geometry consists of perpendicular channels that have opposing inlet and outlet streams, generating a stagnation point where the channels intersect. At the stagnation point the local velocity is zero, and the surrounding streamlines form a planar elongational flow that is directed towards the outlet channels. In the present study, the diameter of the filament is an order of magnitude smaller than the dimensions of the cross slot so that a uniform extension is assumed. Stagnation-point geometries have been shown to produce large Hencky strains, allowing for the uncoil of flexible macromolecules (Feng and Leal 2000; Hudson et al. 2004; Lee et al. 2007; Dylla-Spears et al. 2010; Haward et al. 2012). The cross-slot design was fabricated to be similar to the one that was proposed by Haward et al. (2012), such that corners were added to help "self-lubricate" the flow, minimizing shearing effects at the walls. Here, the "continuous phase" describes the fluid that assists in forming, transporting, and extending droplets of the immiscible "dispersed-phase" sample. Poly(ethylene oxide) (PEO) ($M_w = 7 \times 10^6$ g/mol) was selected as the working polymer, as it has been well characterized in the literature, and it has been used to observe the effects of viscoelasticity on droplet formation and splitting at a T-junction (Link et al. 2004; Husny and Cooper-White 2006; Christopher and Anna 2009). For the majority of the droplet-breakup trials, a 200 mPa·s silicone oil was used as the outer continuous phase fluid. More information regarding the selection of the continuous- and dispersed-phase fluids is discussed in "Selection of continuous- and dispersed-phase solutions".

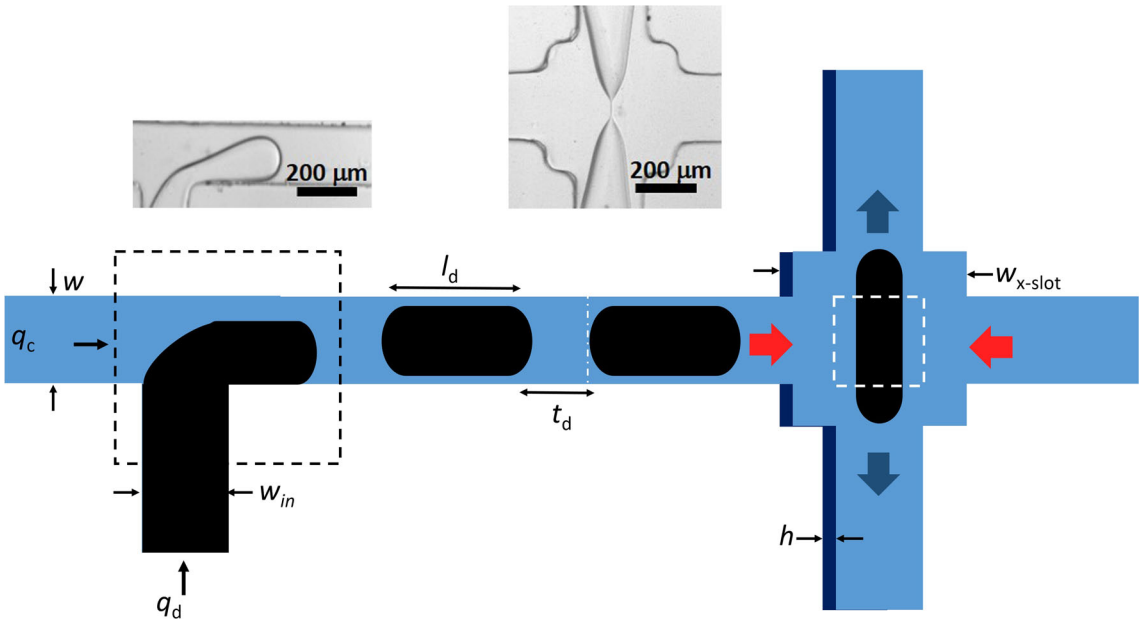

Fig. 1 An overall schematic of the cross-slot device, including the continuous- and dispersed-phase inlet channels with widths of w and w_{in}, respectively. The length, ℓ_d, and time-spacing, t_d, between droplets were controlled by adjusting the ratio of the continuous- and dispersed-phase flow rates, q_c/q_d. The height of the device, h, was similar in magnitude to the width of the channels. The width of the cross slot, w_{x-slot}, was greater than the width of the channels, minimizing wall effects. Images of droplet formation at the T-junction and droplet breakup in the cross-slot geometry are also included

Device fabrication

PDMS was chosen as a substrate for the transparency, ease of fabrication, and cost considerations of the material. Standard photolithography and soft lithography were performed to fabricate the devices.

Photolithography

For performing photolithography, photomask designs were created using SOLIDWORKS® 2D CAD software and produced by CAD/Art Services, Inc. To prepare the master mold, a MicroChem SU-8 2100 negative photoresist was patterned onto a silicon wafer. To improve the adhesion of the photoresist, the surface of the silicon wafer was plasma cleaned (XEI Scientific Evactron™ Decontaminator) for approximately 2 min prior to being spun onto the surface of the wafer. The photoresist was spun, baked, exposed, and developed according to SU-8 2100 processing guidelines provided by MicroChem Corp. (n.d.).

Soft lithography

For soft lithography, a Dow Corning Sylgard® 184 silicone elastomer kit was used with a 1:10 ratio of base to curing agent, as recommended by Dow Corning. The elastomer was then placed under vacuum to remove any excess air bubbles that were generated from the reaction of the base and curing agent. Once any air bubbles had been removed, the PDMS was carefully poured over the silicon master, covering the SU-8 pattern. The wafer was then placed in a vacuum oven at 70 °C for at least 1 h. Once cured, the PDMS was peeled from the silicon master to avoid damaging the SU-8 pattern. To close the channels, a second sheet of PDMS was made on a smooth surface. The two pieces of PDMS were then placed in an oxygen plasma etcher (XEI Scientific Evactron™ Decontaminator) for 3 min and firmly pressed together to irreversibly bond the surfaces. Devices were then baked overnight at 70 °C to allow the channels to regain hydrophobicity. The second piece of PDMS was used to ensure uniform wetting of the channels. A detailed protocol for soft lithography is provided by Friend and Yeo (2010).

Experimental setup

PRIMER

The resulting PRIMER device contained rectangular channels, having a continuous-phase inlet width, w, and a dispersed-phase inlet width, w_{in}, of approximately 200 μm, and a cross slot, consisting of a 400-μm × 400-μm opening with rounded corners. The height, h, of the channels, determined using a Zygo ZeScope™, was approximately 176 μm, which is similar to the width of the device channels ($h/w \approx 1$). A schematic of the overall PRIMER device is presented in Fig. 1, including images of the actual device geometries.

An NE-1002X Programmable Microfluidics syringe pump and an Orion Sage™ M361 syringe pump were used to control the volumetric flow rates in the device in the range of 0.01–1 ml/h. When using higher-viscosity fluids, lower flow rates were required to prevent any leaking from the device that was induced by back pressure. Prior to use, all channels were primed with continuous phase to pre-wet the channel walls.

At the cross slot, images were captured at a rate of 1265 fps with a pixel resolution of 800 pixels × 600 pixels using a Phantom® V4.1 high-speed camera and a Nikon Eclipse Ti-S inverted microscope with a 40× magnification (N.A. = 0.6). Once entering the cross slot, droplets were tracked until a breakup event was complete. Image analysis was performed using a custom-built MATLAB® script to extract the evolution of the filament diameter as a function of time.

Dripping-onto-Substrate

For comparison with a standard measurement of extensional rheology, the short relaxation times and low zero-shear viscosities make using the CaBER impractical for many of the samples. Thus, less traditional technique deemed dripping-onto-substrate (DoS) was used for comparison. Dispersed-phase samples were evaluated using the DoS technique that was presented by Dinic et al. (2015, 2017), reminiscent of other techniques that have used extended liquid bridges in the literature (Bazilevsky et al. 2011). Similar to the CaBER, this technique uses capillary breakup to evaluate the extensional properties of a sample. However, by slowly dispensing the sample from the tip of a needle until it touches the surface of a substrate, the formation of a liquid bridge eliminates the need for a finite step-strain, providing increased sensitivity at low viscosities, when the extensional relaxation time of the material is on the order of the startup time of the CaBER. If a substrate is chosen so that the sample wets the surface, a uniform filament emerges that breaks in a finite amount of time, driven by dominating capillary forces. For the present work, a DoS device was built in-house. Videos were captured at 1265 fps at a pixel resolution of 800 pixels × 600 pixels, using the Phantom® V4.1 high-speed camera attached to a 130-mm extension tube and a 10× objective. Videos were processed using a custom-built MATLAB® script that tracked the diameter of the filament in time. In the present study, results from the DoS measurements were used as a comparison for the data that was collected using the PRIMER device.

Selection of continuous- and dispersed-phase solutions

Dispersed phase

For testing and validating the device, two types of dispersed-phase solutions were used. The first type of dispersed-phase solution consisted of high-molecular-weight ($M_w = 7 \times 10^6$ g/mol) poly(ethylene oxide) (PEO) that was dissolved in deionized water (DIW). The second type of dispersed-phase solution that was tested consisted of glycerol (GLY) that was dissolved in deionized water (DIW) to produce Newtonian fluids that have similar zero-shear viscosities to the PEO solutions that were tested. A summary of the dispersed-phase solutions is provided in Table 1, which includes an indication of the limit of quantification ($<$ loq) when a filament was observed to form but the relaxation time fell below the limit for the current PRIMER setup. Given the capture rate of 1265 fps while assuming that a minimum of five frames are needed to fit a decay profile, this limit was estimated to be 4 ms. For comparison (see "Viscoelasticity of the dispersed phase"), the Zimm relaxation time was found to be 2.6 ms, and the minimum observable concentration was found to be $c_E = 8$ ppm.

To prepare the aqueous PEO solutions, a 5000 ppm stock solution was made by dissolving Dow Chemical Company POLYOX™ WSR 303 in DIW and slowly rolling the solution at room temperature to allow for homogenization. According to Graessley (1980), c* can be evaluated as

$$c^\star \approx \frac{1}{[\eta]}. \tag{11}$$

The Mark-Houwink-Sakurada (MHS) relationship was used to evaluate the critical overlap concentration, $c^\star$, for PEO in deionized water (DIW) according to the relationship

$$[\eta] = K[M_v]^a, \tag{12}$$

where $[\eta]$ is the intrinsic viscosity and M_v is the volume-average molecular weight. The parameters K and a depend on the polymer/solvent system, which can be found in a handbook for common polymers (Brandrup et al. 1989). In addition, Tirtaatmadja et al. (2006) determined the intrinsic viscosity to follow the equation, $[\eta] = 0.072 M_w^{0.65}$, where M_w is the weight-average molecular weight, for various studies using PEO in the literature. We used the manufacturer's reported value for the weight-average molecular weight ($M_w = 7 \times 10^6$ g/mol) to find the critical overlap concentration to be $c^\star = 4.9 \times 10^{-4}$ g/cm^3. The stock solution, which was evaluated to have a concentration of approximately 13 times $c^\star$, was diluted as necessary to ensure that the samples were in known concentration regimes. Dilutions were made to create solutions with concentrations of 10, 50, 100, and 500 ppm ($c/c^\star \approx 0.03, 0.1, 0.3, 1$, respectively). All solutions were prepared at room temperature and allowed to equilibrate for 48 h prior to use. Samples were stored in amber glass bottles under nitrogen to prevent degradation to the polymer.

To characterize the shear rheology of the dispersed-phase solutions, the samples were tested using a TA Instruments AR-G2 rotational rheometer that was equipped with a 60-mm, 1° cone and a Peltier plate. For the 10 to 500 ppm solutions, the samples did not appear to shear thin over the reliable range of shear rates that were tested $\left(10 - 10^3 \frac{1}{s}\right)$, and they had shear viscosities that were on the same

Table 1 A summary of the dispersed-phase solutions that were tested in the PRIMER device, including viscoelastic solutions composed of poly(ethylene oxide) (PEO) in deionized water and Newtonian glycerol (GLY)/water solutions

Poly(ethylene oxide) in water				
Composition	$c/c^\star$	η_0 ($T = 25$°C)	DOS λ_E	PRIMER λ_E
[ppm]		[mPa·s]	[ms]	[ms]
5000	13	200	205	194±49
500	1	1.2	4	6±3
100	0.3	0.96	$<$ loq[a]	$<$ loq
50	0.1	0.95	$<$ loq	$<$ loq
10	0.03	0.90	–[b]	–
Glycerol in water				
Composition	$c/c^\star$	η_0 ($T = 25$°C)	DOS λ_E	PRIMER λ_E
[wt%]		[mPa·s]	[ms]	[ms]
90	–	164	–	–
80	–	43	–	–
10	–	1.2	–	–

[a]Relaxation time falls below the current limit of quantification

[b]Filament was not formed during the droplet-breakup event

order of magnitude ($\eta_0 \sim 1$ mPa·s) (Fig. 2). For the stock solution (5000 ppm), shear-thinning behavior was noted over the range of shear rates that were tested (Fig. 2). Fitting the data from the plot of viscosity versus shear rate, the zero-shear viscosity of the stock solution was evaluated to be approximately $\eta_0 = 200$ mPa·s, which was two orders of magnitude greater than the solutions at concentrations between 10 and 500 ppm. The flow behavior of the stock solution was thus dominated by the presence of entanglements.

Continuous phase

In selecting continuous-phase fluids to be used, choosing fluids that preferentially wet the surface of the PDMS channels relative to the dispersed phase was important to ensure that the disperse-phase sample would not be attracted to the channels. The degree of wetting (wettability) of the continuous phase is known to be an important factor in the droplet formation process, and it could interfere with the droplet-breakup event, if not considered appropriately (van Steijn et al. 2010). To better quantify the influence of the continuous-phase fluid on the droplet-breakup and filament-formation processes, standards of silicone oils over a range of shear viscosities ($30 - 500$ mPa·s) from Brookfield and Dow Corning were tested.

For the present work, the interfacial tensions between the continuous- and dispersed-phase fluids were assumed to have values on the same order of magnitude ($\sigma \approx 30 \frac{mN}{m}$) as reported literature values (Christopher and Anna 2009). This assumption simply means that the Weber number is assumed to be very small ($We \ll 1$), such that the process is "self-thinning," as discussed in the section on Relevant Dimensionless Parameters. We will revisit this applicability of this assumption in the Conclusions. Note that, when the process is "self-thinning," the interfacial tension is not used in any calculations for the characteristic extensional relaxation time, as the extensional strain rate is only a function of the extensional relaxation time itself (see discussion of Eq. 9).

Results and discussion

We explored the effects that viscous and elastic stresses have on a droplet-breakup event that occurs in the cross slot. For this aim, a number of experiments were performed that varied the ratio and magnitude of the flow rates into the device of the continuous and dispersed phases as well as the types of continuous and dispersed phases that were employed.

Droplet breakup for Newtonian and viscoelastic fluids

As droplets entered the cross-slot geometry, their shapes become altered so that the droplets were elongated towards the outlet channels. Reaching the stagnation point, droplets either extended and broke into two segments or remained intact, exiting one of the two outlet channels. Conditions that define when a droplet-breakup event will occur have been discussed extensively in the literature (Link et al.

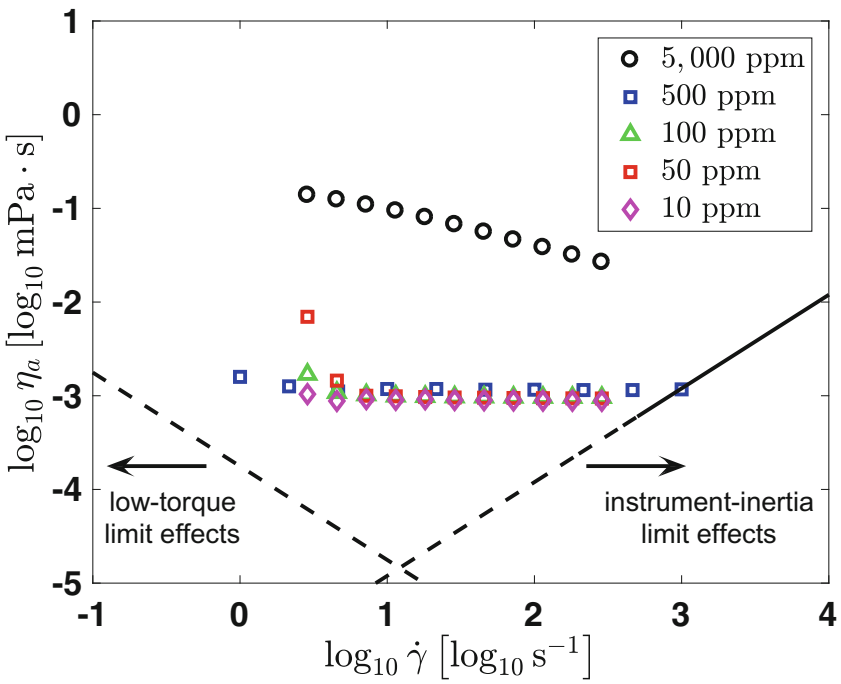

Fig. 2 Apparent shear viscosity (η_a) versus shear rate ($\dot{\gamma}$) for the solutions of PEO ($M_w = 7 \times 10^6$ g/mol) at 10, 50, 100, 500, and 5000 ppm that were tested using the cross-slot microfluidic device. Shear characterization was performed at 25 °C with a 60-mm, 1° cone and plate. The black dashed lines indicate where low-torque (left limits) and inertial effects (right limits) may lead to errors in measurement, evaluated according to Ewoldt et al. (2015)

2004; Christopher and Anna 2009). Specifically, operating diagrams depicting under what condition droplets break and do not break at T-junctions have been presented. In these diagrams, relevant parameters for the breaking of droplets include the capillary number, Ca, and the initial aspect ratio of the droplet, $\chi = \frac{\ell_d}{\pi w}$. Consistent with the Plateau-Rayleigh instability for the breakup of a cylindrical thread, an extended droplet can minimize its surface area by splitting. In agreement with results that have been reported in the literature, droplets in the present study were more likely to break for larger capillary numbers (higher flow rates) and higher aspect ratios (longer droplets) (Link et al. 2004).

Typical droplet-breakup profiles at the cross slot for Newtonian and viscoelastic fluids are presented in Fig. 3. The main discrepancy between the two profiles is that the formation of a filament was clearly observed for the breakup of the viscoelastic droplet of 500 ppm PEO solution that is shown in Fig. 3b and was not apparent for the Newtonian GLY/DIW solution that is shown in Fig. 3a. Furthermore, for viscoelastic droplets, the well-known beads-on-a-string morphology (also known as pearling) was observed at late times in the breakup process (Li and Fontelos 2003; Oliveira and McKinley 2005; Clasen et al. 2006a; Christopher and Anna 2009; Bhat et al. 2010). Newtonian fluids, on the other hand, appeared to form satellite droplets with no noticeable connecting threads.

Monitoring the diameter of a droplet of the 5000 ppm PEO solution at a range of points along the profile of the droplet (Fig. 4), four distinct regimes were noted. The physics that dominate each regime can be described by the associated forces, including drag forces, F_D, viscous forces, F_η, elastic forces, F_E, and capillary forces, F_C. Balances of the dominating forces include (i) $\left[F_D \sim F_\eta\right]$ the early stretching and necking of the droplet as it reached the stagnation point, (ii) $\left[F_C \sim F_\eta\right]$ a rapid decrease in the diameter that was driven by dominating capillary forces, (iii) $[F_C \sim F_E]$ an elastocapillary regime where the growth of elastic stresses overcame the viscous stresses and balanced with the capillary pressures that continued to drive the breakup process, and (iv) the formation of the beads-on-a-string morphology. In the present study, the third and fourth regimes were found to be unique to viscoelastic samples, as Newtonian fluids did not appear to form appreciable filaments over the range of shear viscosities that were tested. The regime of interest for the present study was the elastocapillary regime (iii), where the elastic properties of a material could be extracted.

Over the first three regimes, results appeared insensitive to the vertical position along the filament where the

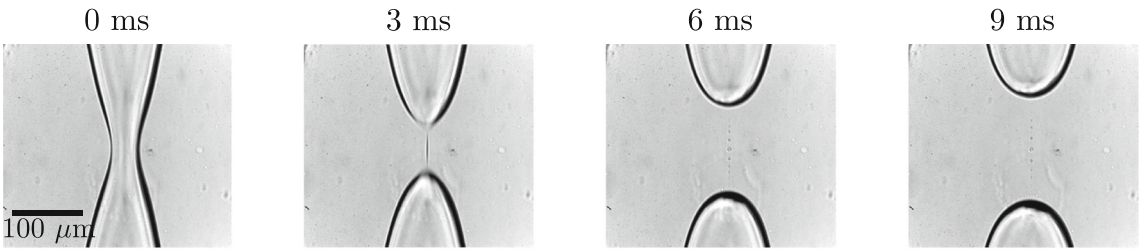

(a) Newtonian 10-wt% glycerol.

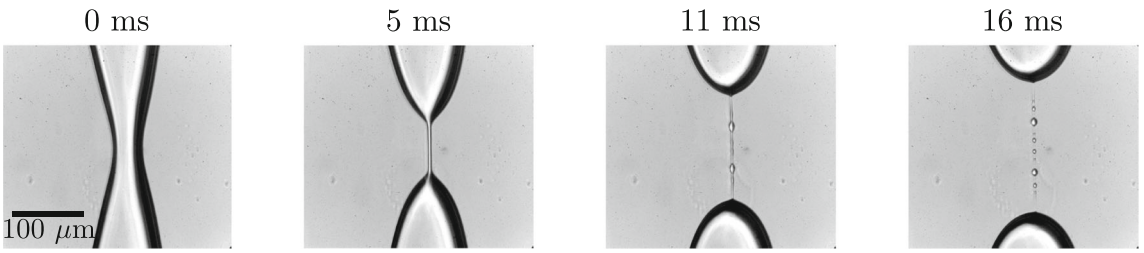

(b) Viscoelastic 500-ppm PEO.

Fig. 3 Droplet breakup of Newtonian and viscoelastic fluids in the cross-slot geometry of the PRIMER device. At a time of $t = 0$ ms, capillary pressures initiate the droplet-breakup event. **a** A 10 wt% glycerol/water solution rapidly decays in time. Satellite droplets are observed at late times, and depending on the viscosity of the glycerol/water solution, the number and size of these satellite droplets varied. **b** A 500 ppm PEO/water solution forms a cylindrical filament that decays in time. At late times, the well-known beads-on-a-string morphology was observed, and depending on the concentration of PEO, the size of the initial filaments and the structure of the beading patterns varied. Images were enhanced for visualization

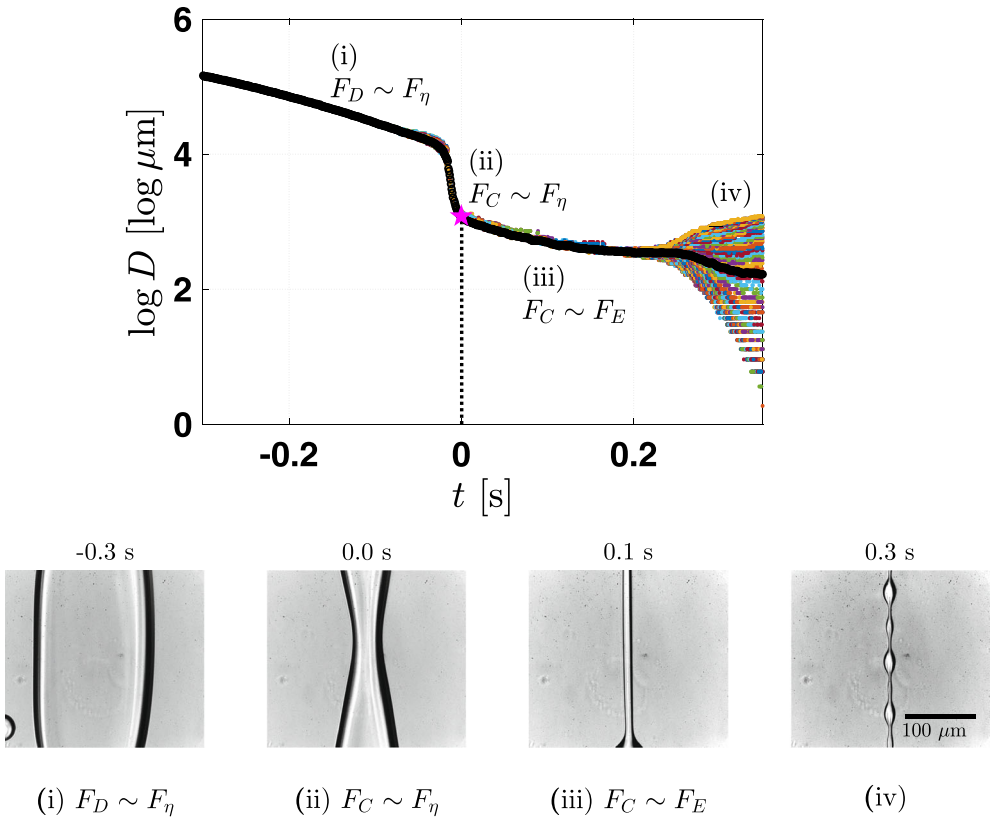

Fig. 4 Diameter-decay profiles for one trial of a droplet of 5000 ppm PEO stock solution for a range of pixels along the profile of the filament. The black line represents the average values of the diameter over this range. Four distinct regimes are noted including (i) the early stretching and necking of the droplet as it reached the stagnation point causing capillary pressures to grow, (ii) a rapid decrease in the diameter that was caused by dominating capillary forces after a critical diameter is reached, (iii) an elastocapillary regime where the growth of elastic stresses balances the capillary pressures driving the breakup process, and (iv) the formation of the beads-on-a-string morphology. The initial time ($t = 0$ s) is the time at the end of regime (ii) in which a filament forms, which is highlighted by a pink star on the plot. Images of the morphology of the droplet at each regime are included below the plot. The physics that dominate each regime, including drag forces, F_D, viscous forces, F_η, elastic forces, F_E, and capillary forces, F_C, are also shown

measurement was taken, as exemplified in Fig. 4. The fourth regime, however, was apparent by the "fanning" of the decay profile, as beads of alternating sizes were formed. Iterated stretching is known to occur in the late-time thinning dynamics for finitely extensible polymer solutions, where the neck that connects a thread to a primary drop becomes unstable (Oliveira and McKinley 2005). This process leads to the formation of secondary-, tertiary-, and higher-generation droplets. In the present study, the size and generation of bead growth depended on the concentration and type of polymer. Although finite extensibility dampens the instability at long times, literature suggests that measuring the steady growth of the transient extensional viscosity is possible by monitoring the slow capillary-driven thinning between beads (Oliveira and McKinley 2005; Oliveira et al. 2006). However, the filaments between beads were too small to detect with the experimental setup that was used in the present work.

Comparison of the DoS and PRIMER techniques

To initially validate the use of a droplet-breakup event for extracting extensional measurements, a 5000 ppm PEO solution was tested using both the dripping-onto-a-substrate (DoS) and the droplet breakup at a cross-slot (PRIMER) techniques. A more concentrated polymer solution was initially selected to ensure that comparisons could be made using both techniques. The results of ten droplet-thinning profiles using PRIMER were then averaged and compared with the evolution profiles of the filaments that were formed using the DoS technique.

In anticipation of leveraging Eq. 8, the natural logarithm of the resulting diameter-decay profiles from the decays of the 5000 ppm PEO solutions is plotted in Fig. 5. Both the DoS and the PRIMER techniques show similar trends in filament-thinning profiles. The diameter at $t = 0$ s, D_1, is the diameter of the initial filament that was formed at the

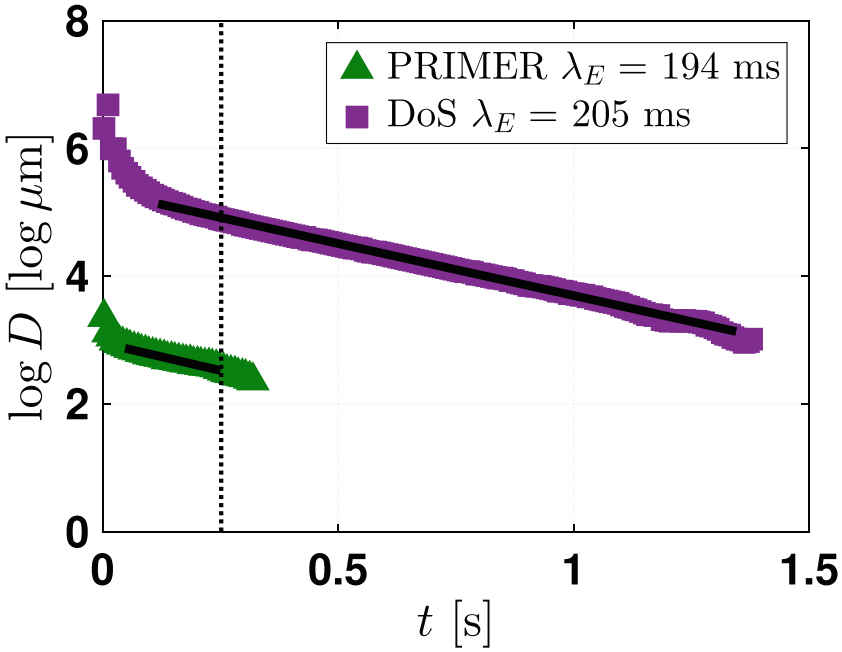

Fig. 5 A comparison of diameter-decay profiles for a 5000 ppm PEO stock solution using PRIMER and DoS techniques. For the PRIMER results (green triangles), a 200 mPa·s silicone oil was used as the continuous-phase fluid. The solid lines represent the linear fits of the elastocapillary regime of interest, where extensional relaxation times were extracted. The dashed line represents the time in which the onset of beads-on-a-string was observed during the droplet-breakup event in the PRIMER device

end of regime (ii). For the DoS method, the initial filament diameter was orders of magnitude larger than the filaments that were formed in the cross slot. A more general curve for this particular experiment can be formed by simply plotting the natural logarithm of the ratio of the diameter to the initial diameter $\left(\log \frac{D(t)}{D_1}\right)$ versus time (t), which would cause the trends to be indistinguishable prior to the onset of regime (iv). Further, if the abscissa is scaled by the extension relaxation time, a plot of $\left(\log \frac{D(t)}{D_1}\right)$ versus time $\left(\frac{t}{\lambda_E}\right)$ would provide the same trend for all materials going through capillary breakup in the elastocapillary regime (iii).

Regime (iii) was nearly three times longer in the DoS technique than in the PRIMER, allowing the dynamics of interest to be more easily captured. The dashed line in Fig. 5 represents the onset of regime (iv), which impacted our ability to observe regime (iii) using the PRIMER technique. Thus, macroscopic CaBER measurements have been successfully conducted with cameras with standard frame rates, such as a smartphone (Marshall et al. 2017), while the microscopic measurements require high-speed cameras to obtain enough information for data analysis before the onset of regime (iv).

To extract information from the diameter-decay profiles for both PRIMER and DoS, an analysis was performed in the same manner as in CaBER experiments, yet subtle differences in the procedures need to be explicitly described. Similar to CaBER techniques, the extensional techniques that are presented are not completely shear free, and they can be sensitive to the shear history. In the PRIMER device, the filament continues to stretch as it enters the outlet channels of the cross-slot geometry. Nevertheless, when exponential thinning of the filament occurs, an extensional relaxation time can generally be extracted according to Eq. 8.

For the present experiments, despite the 5000 ppm PEO fluid being concentrated, the natural logarithm of the diameter-decay profiles that are observed in Fig. 5 appears to have linear elastocapillary regimes that are highlighted by the solid lines. The characteristic extensional relaxation times were evaluated using the slopes of the fitted curves, where the slope is inversely proportional to the characteristic extensional relaxation time. When evaluated, the relaxation times from the two techniques were found to be in good agreement, with an extensional relaxation time of 205 ± 20 ms found using the DoS technique and an extensional relaxation time of 194 ± 49 ms found using ten trials of the PRIMER technique. Errors are given at one standard deviation.

Viscoelasticity of the dispersed phase

Since the splitting of droplets could serve as a means of characterizing low-viscosity elasticity, the dynamics at lower concentrations of polymer were explored. Figure 6 presents data that was collected for dilutions of the stock solution at 10, 50, 100, and 500 ppm. Filament formation was observed to be less pronounced at lower concentrations of polymer. The lowest concentration in which a filament was observed was 50 ppm. However, using our current camera system, the number of frames that were available was too low to fit a decay profile at concentrations below 500 ppm. At 500 ppm, the extensional relaxation time that was measured was approximately 6±3 ms, in agreement

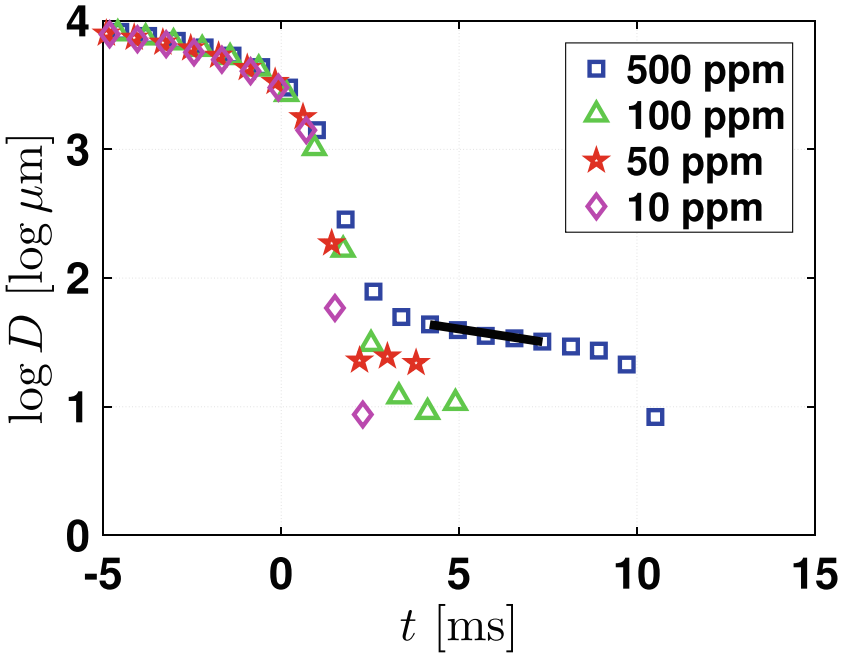

Fig. 6 Diameter-decay profiles for filaments at concentrations of PEO of 10, 50, 100, and 500 ppm. The natural logarithm of the diameter is plotted versus time. Only the 500 ppm solution had an elastocapillary regime that could be fit

with the relaxation time that was determined by DoS as well as values that have been reported in the literature (Dinic et al. 2015). For the CaBER, the 500 ppm solution would be near, or fall below, the lower limit of measurability.

When characterizing solutions that have lower concentrations, the initial size of the filament decreased, and the beading profiles were altered, as seen in Fig. 7. Furthermore, the "strings" that were connecting the beads were difficult to discern, as their diameter neared the Abbe diffraction limit for optical detection.

Although the present work draws attention to the elastocapillary number, Ec, Clasen et al. (2006b) discuss that, for an elastocapillary number that is greater than unity ($Ec > 1$), the filament-thinning process may not be observed if a minimum observable concentration, c_E, is not achieved. The minimum concentration that is required for observing any viscoelastic effects was found to be

$$c_E = \frac{3}{2}\frac{M_w \eta_s}{RT\lambda_z L^2}, \tag{13}$$

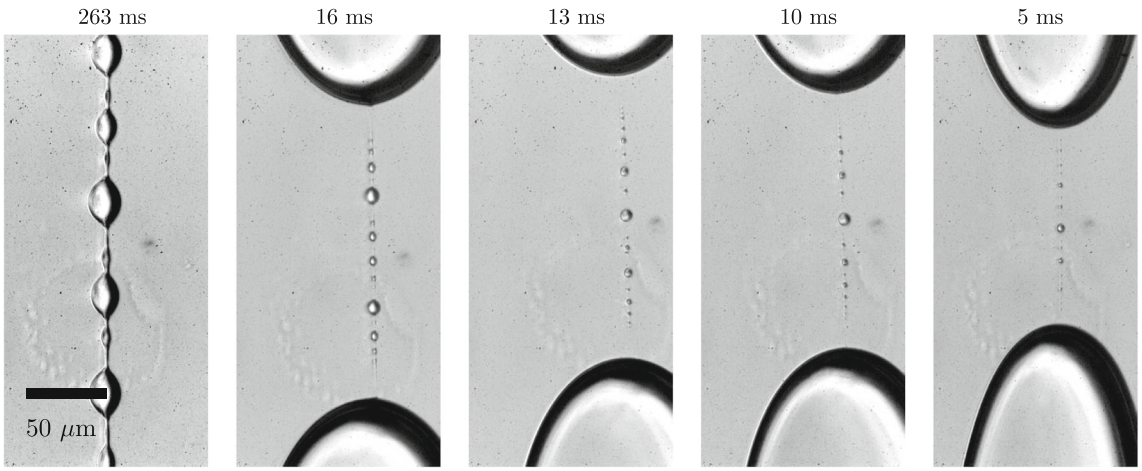

(a) $c = 5,000$ ppm (b) $c = 500$ ppm (c) $c = 100$ ppm (d) $c = 50$ ppm (e) $c = 10$ ppm

Fig. 7 Beading profiles for filaments of PEO solutions at concentrations **a** 5000, **b** 500, **c** 100, **d** 50, and **e** 10 ppm that are dispersed in 200 mPa·s silicone oil. As the concentration decreases, the initial size of the filament decreased, and the beading profiles were altered

where M_w is the weight-averaged molecular weight of the polymer, η_s is the solvent viscosity, R is the ideal gas constant, T is the temperature, λ_z is the Zimm longest relaxation time of the polymer, and L describes the finite extensibility of the polymer. Below this concentration, the fully extended polymer carries less stress than the solvent, causing viscous stresses to dominate elastic stresses in resisting filament thinning.

For dilute polymer solutions, the total solution relaxation time is proportional to the relaxation time of a single polymer molecule. Although the polymer may have multiple mechanisms of relaxing, a longest relaxation time can often be used to describe the magnitude of the overall process. The longest relaxation time in Zimm theory can be approximated by

$$\lambda_z \cong \frac{[\eta] M_w \eta_s}{\zeta(3\nu) N_A k_B T}, \tag{14}$$

such that N_A is Avogadro's number, k_B is the Boltzmann constant, and $[\zeta(3\nu)]^{-1}$ is a coefficient that depends on the solvent/solute system (Tirtaatmadja et al. 2006; Öttinger 2012). This coefficient corrects for hydrodynamic interactions, and it can be evaluated as $[\zeta(3\nu)]^{-1} = \sum_{i=1}^{\infty} i^{-3\nu}$, where ν is the Flory exponent that describes the excluded volume of a polymer chain (Flory 1953; Teraoka 2002). Zimm theory describes the hydrodynamic interactions between the solvent and the beads of a Gaussian chain, and it is often used as a comparison for describing the relaxation times of dilute polymer solutions (Christopher and Anna 2009; Clasen et al. 2006b).

For the present work, for a dilute PEO solution in water ($\eta_s = 1$ mPa·s) at room temperature ($T = 25$ °C), it has a Zimm relaxation time that is estimated to be approximately 2.6 ms. Thus, for small deformations of the PEO solutions studied herein, we can expect the reported relaxation times to be near this value. At large deformations, however, other characteristic times may be observed that deviate from the Zimm relaxation time (Clasen et al. 2006b).

Following the process performed by Tirtaatmadja et al. (2006) and Christopher and Anna (2009), the finite extensibility parameter of the PEO solutions can be calculated by using the following equation

$$L^2 = 3N_K, \tag{15}$$

where N_K is the number of Kuhn segments in the chain and is evaluated as

$$N_K = \alpha \left[\frac{\left[\sin\left[\frac{\theta}{2}\right]\right]^2}{C_{\infty_{mod}}} \right]^{\frac{0.5}{(1-\nu)}}. \tag{16}$$

In Eq. 16, $\alpha = 3M_w/M_0$ is the number of bonds per chain in which M_0 is the molecular weight of the repeating monomer unit, and θ is the carbon-carbon bond angle ($\theta = 109.5°$). The repeat unit for poly(ethene oxide) [-CH_2CH_2O-] has a molecular weight of $M_0 = 44$ g/mol. The modified characteristic ratio $C_{\infty_{mod}}$ accounts for the effects of the solvent quality. Tirtaatmadja et al. (2006) reported values of $C_{\infty_{mod}} = 4.01$ and $\nu = 0.55$. Using these values with Eq. 16, the finite extensibility parameter is found to be $L^2 \approx 1.9 \times 10^5$, which is the same order of magnitude as values found for similar PEO solutions described in the literature (Christopher and Anna 2009).

Returning to Eq. 13, the minimum observable concentration for the PEO solutions that were used in the present study was evaluated to be approximately $c_E = 8$ ppm. Although all dilutions that were tested were above the calculated minimum observable concentration, measurements were unsuccessful for solutions of 100 ppm and below with the current setup.

Assumption of "self-thinning" breakup

We can now return to the assumption that a sufficient interfacial tension is present to be in the "self-thinning" regime, where the Weber number is small ($We \ll 1$). We can make a scaling argument for the limitations of the technique by assuming the characteristic velocity (u^*) in Eq. 6 is equal to the extensional strain rate ($\dot{\varepsilon}$) times the characteristic length scale (ℓ^*). We can substitute the self-thinning Weissenberg number to find the self-thinning extensional strain rate to be $\dot{\varepsilon} = \frac{2}{3\lambda_E}$, such that

$$We = \frac{\rho \dot{\varepsilon}^2 \ell^{*3}}{\sigma} = \frac{4\rho \ell^{*3}}{9{\lambda_E}^2 \sigma} \ll 1. \tag{17}$$

Now, since we have a range of characteristic extensional relaxation times, we can assume the largest characteristic length scale $w_{\text{x-slot}} = 400$ μm in the device to solve for a required interfacial tension. If we assume that the extensional relaxation time is equal to the limit of quantification ($\lambda_E = 4$ ms) as discussed earlier, the density of water $\left(\rho = 1 \frac{\text{g}}{\text{cm}^3}\right)$ will yield a critical interfacial tension of $\sigma_c = 1.8 \frac{\text{mN}}{\text{m}}$. Thus, as long as the interfacial tension is greater than this value, the system can be assumed to be in the "self-thinning" regime, which was true in this case ($\sigma \approx 30 \frac{\text{mN}}{\text{m}} \gg \sigma_c$).

This analysis can also be used to estimate realistic limitations of the technique. As the characteristic extensional relaxation time decreases, the critical interfacial tension will increase $\left(\sigma_c \sim {\lambda_E}^{-2}\right)$, and as the characteristic length scale decreases, the critical interfacial tension will decrease $\left(\sigma_c \sim \ell^{*3}\right)$. Thus,

$$\lambda_E \gg \frac{2}{3}\left[\frac{\rho}{\sigma}\right]^{\frac{1}{2}} \ell^{*\frac{3}{2}} = \lambda_c, \tag{18}$$

where λ_c is the critical extensional relaxation time of the technique. Assuming that the limitation of a bright-field

microscopy is an initial filament diameter of $D_1 = 1\ \mu$m, a reasonable interfacial tension of $\sigma = 44\ \frac{\text{mN}}{\text{m}}$ will limit the critical extensional relaxation time to $\lambda_c = 0.1$ ms. If you assume the limitation of dark-field microscopy is an initial filament diameter of $D_1 = 0.1\ \mu$m, the critical extensional relaxation time becomes $\lambda_c = 3 \times 10^{-3}$ ms.

Droplet-breakup response to changes in flow rate and continuous phase

Although the results of the DoS and PRIMER techniques were consistent, testing how sensitive the PRIMER technique is to varying experimental conditions such as the flow rate, the dispersed-phase fluid, and the continuous-phase fluid was necessary to establish robustness.

To explore how varying flow conditions will impact the dynamics of droplet breakup in a cross-slot geometry, droplets of the 5000 ppm PEO stock solution were tested using a variety of continuous-phase oils varying between 30 and 500 mPa·s at flow rates varying from 0.01 to 1 ml/h. Figure 8 contains a plot of the raw diameters versus time for droplets splitting in the 200 mPa·s silicone oil. The elastocapillary regime (iii) appeared relatively unaffected by the flow conditions as compared with early times (regime i), where the stretching of the droplet occurs. As the overall flow rates in the cross slot are increased (i.e., the sum of the flow rates of the continuous and dispersed phase, $Q = q_c + q_d$, the drag that acted on a droplet was more substantial, which caused the droplet to elongate more rapidly, reflected by the steepening of the slope at early times in Fig. 8. Further analysis reveals that a linear relationship exists between the total volumetric flow rate and the magnitude of the slope of the decay profiles in this regime for a single continuous- and dispersed-phase combination. More experimentation is required to elucidate how this linear relationship is impacted by the viscosity and interfacial tension of the continuous and dispersed phases. In terms of the elastocapillary regime, the evaluated extensional relaxation times fall within the same order of magnitude as the DoS trials (Table 2).

Table 2 A summary of the continuous- and dispersed-phase flow rates that were tested for the 5000 ppm stock solution that was dispersed in the 200 mPa·s in the PRIMER

q_c [ml/h]	q_d [ml/h]	λ_E [ms]
0.13	0.04	170
0.13	0.02	240
0.73	0.04	180
0.73	0.03	150
0.05	0.01	220

Since the diameter of the initial filament ($\sim 10\ \mu$m) is much less than the characteristic length of the cross slot, the elastocapillary regime is assumed to be less affected by global flow conditions. To validate this assumption, the size of the droplets and the capillary number were varied. Figure 9 contains the results for these trials. The filled-black markers represent varying continuous-phase viscosity at a fixed flow ratio, $q_d/q_c = 0.8$. Unlike results from the passive breakup of droplets at a T-junction, the extensional relaxation times that were characterized did not appear to be greatly influenced over the range of experimental conditions

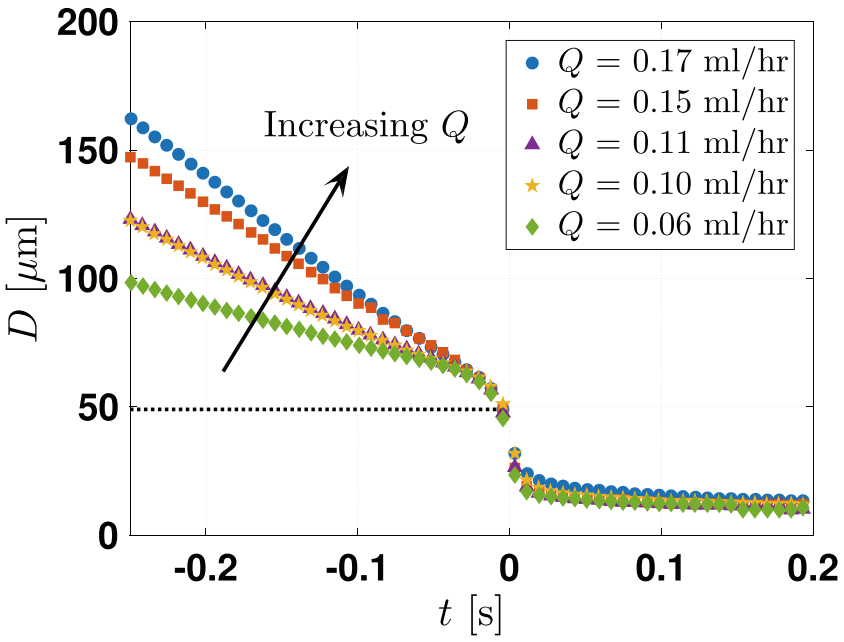

Fig. 8 A plot of the diameter versus time for varying overall volumetric flow rates ($Q = q_d + q_c$) for a stock solution of 5000 ppm PEO that was dispersed in 200 mPa·s silicone oil. The slope of the initial viscous-drag regime (regime i: $F_D \sim F_\eta$) increased as the overall flow rates in the device were increased

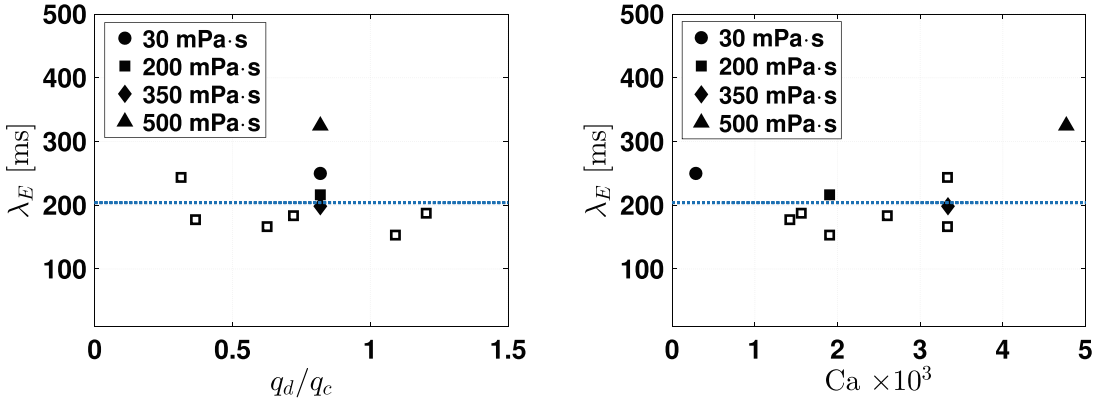

(a) Flow ratio.

(b) Capillary number.

Fig. 9 Results for trials that vary the size of the droplets, a function of the ratio of the flow rates of the dispersed phases to the continuous phase, q_d/q_c, and the capillary number, a function of continuous-phase velocity, u_c, and the continuous-phase viscosity, η_c, using the 5000 ppm PEO. **a** The extensional relaxation time is plotted versus the ratio of the dispersed- and continuous-phase flow rates. **b** The extensional relaxation time is plotted versus the capillary number. The filled-black markers represent varying continuous-phase viscosity at a fixed flow ratio, $q_d/q_c = 0.8$. Four symbols are used to represent four different outer continuous phases with viscosities of 30, 200, 350, and 500 mPa·s. The blue-dotted lines represent the relaxation time that was characterized in the DoS trial

that were tested. Furthermore, although some variability existed, no systematic cause for the variability was noted, and all of the approximate extensional relaxation times fell within the range of the values that were calculated by the DoS technique. Relaxation times for droplet breakup at a T-junction have been found to be influenced by the capillary number and the initial aspect ratio (Christopher and Anna 2009). In those experiments, the initial capillary numbers were greater than 10^{-2}, whereas in the present experiments, the capillary numbers were maintained below this value. When capillary forces dominate over viscous stresses, we assume that the breakup event will be less influenced by the surrounding continuous-phase flow.

Conclusions and future work

In the present study, droplet breakup in the cross slot of a microfluidic device was presented as a means of characterizing weakly-viscoelastic fluids. Since the length scales that are associated with such devices are on the order of a few microns or less, the effects of elasticity are thought to be more pronounced.

Although the effects of elasticity were clearly observed for a 5000 and 500 ppm PEO solution with a droplet-evolution profile that was similar to the profile that was captured using the DoS technique, attempts to extract a characteristic extensional relaxation time proved to be unsuccessful at more dilute concentrations for the current setup. Successfully measuring the 500 ppm PEO sample, however, proved that the PRIMER has the ability to surpass the capabilities of a standard CaBER.

In addition to the necking and breakup of an extended liquid bridge (Bazilevsky et al. 1990, 2001, 2011; Entov and Hinch 1997; Stelter et al. 2000; Yarin 1993), other techniques that have employed capillary breakup to characterize semi-dilute and dilute polymer solutions include the dripping (Cooper-White et al. 2002; Amarouchene et al. 2001; Basaran 2002; Tirtaatmadja et al. 2006; Wagner et al. 2005) and jetting (Ardekani et al. 2010; Christanti and Walker 2001, 2002; Keshavarz et al. 2015; Sharma et al. 2015; Schummer and Tebel 1982; Schümmer and Tebel 1983) of samples. The Rayleigh Ohnesorge jetting extensional rheometer (ROJER), for example, is a jetting technique that has been demonstrated to achieve extensional relaxation times down to 60 μs (Keshavarz et al. 2015). For the ROJER technique, the breakup of a fluid jet is controlled by imposing perturbations of a known amplitude and frequency. Similar to the CaBER, the evolution of the jet instability is monitored in real time, allowing for the characterization of complex fluids having viscosities on the same order of magnitude as water. Unlike the CaBER technique, however, disadvantages of the ROJER include challenges in optically tracking the evolving filament (Ardekani et al. 2010).

Aside from smaller length scales, additional benefits of the current setup include requiring smaller sample sizes and having an outer continuous-phase fluid that is not open to the atmosphere. For samples that are volatile or easily degraded in air, such a setup is highly desirable.

Although providing flow symmetry similar to the OSCER, the PRIMER does not rely on birefringence to indicate the presence of extensional stresses, instead benefitting from the theory of droplet breakup that allows for ease of measurement. Furthermore, when compared with the recent micro-CaBER technique, the PRIMER allows for the utilization of microscopy techniques (such as dark-field microscopy) that could be further leveraged to approach c_E, the minimum observable concentration.

Identifying performance limitations will be critical to fully exhaust the capabilities of the PRIMER. In some instances with the current setup, the time scale that was associated with the droplet-breakup event was too rapid to be captured. For filaments that form and break on a time scale that is on the order of a millisecond or less, a more capable camera is needed to collect enough data points to fit the elastocapillary regime. Additionally, the onset of the beads-on-a-string instability tended to dampen the duration of the elastocapillary regime of interest. To address this issue, a proper study of the onset of the beads-on-a-string instability in the cross-slot geometry is required. As discussed by Bhat et al. (2010), for systems with larger intrinsic Deborah numbers and Ohnesorge numbers, no beads should be observed. In theory, by reducing the length scale of the system, the values of both of these parameters should increase. Nevertheless, the numerical studies that were presented by Bhat et al. (2010) did not involve a viscous outer fluid. A deeper investigation into how the viscosity of the outer fluid influences the onset of the beads-on-a-string instability is thus imperative for improving the design of the device.

Still, differences between the CaBER and PRIMER are important to distinguish. For example, the CaBER applies a finite step-strain to a material, whereas the PRIMER continues to stretch a sample as the filament thins. Thus, the assumption of a self-thinning filament may not hold if the time scale of breakup is less than the time scale of the external forcing. Again, the Weber number can be used to suggest if the filament-thinning process is self-thinning, as we discussed in detail. To make the cross-slot device more similar to a CaBER, a more advanced pumping system could be employed to actively break droplets, and other geometry configurations could be explored.

For a CaBER-like design, an external forcing would instantaneously extend a droplet and then allow for the self-thinning of the filament. To passively achieve such a process, a droplet could enter into a small cross section that exits into an expansive reservoir, lowering the flow rate of the droplet from the cross-slot region. For a FiSER-like design, to extend the length of the filament at an exponential rate, the shape of the cross-slot geometry could be modified to ensure a constant strain rate.

Acknowledgments The authors would like to thank Dr. Skip Rochefort, Dr. Alex Yokochi, and Dr. Adam Higgins for their contributions to this work. The authors would also like to thank Oregon State University's Johnson Summer Internship program and the Saturday Academy's Apprenticeships in Science and Engineering (ASE) program for supplying talented interns to participate in this work, specifically the authors would like to thank Shelley Haug, Aleesha Liedtke, Katie Moreno, Anika Todt, and Zach Wallace for their assistance in running preliminary experiments. KAM and TWW would also like to thank Hewlett Packard Inc. and the Diversity Pipeline Fellowship at Oregon State University for financial support.

References

Amarouchene Y, Bonn D, Meunier J, Kellay H (2001) Inhibition of the finite-time singularity during droplet fission of a polymeric fluid. Phys Rev Lett 86(16):3558

Anna SL, McKinley GH (2001) Elasto-capillary thinning and breakup of model elastic liquids. J Rheol 45(1):115–138

Anna SL, McKinley GH (2008) Effect of a controlled pre-deformation history on extensional viscosity of dilute polymer solutions. Rheol Acta 47(8):841–859

Anna SL, McKinley GH, Nguyen DA, Sridhar T, Muller SJ, Huang J, James DF (2001) An interlaboratory comparison of measurements from filament-stretching rheometers using common test fluids. J Rheol 45(1):83–114

Ardekani AM, Sharma V, McKinley GH (2010) Dynamics of bead formation, filament thinning and breakup in weakly viscoelastic jets. J Fluid Mech 665:46–56

Arratia PE, Cramer LA, Gollub JP, Durian DJ (2009) The effects of polymer molecular weight on filament thinning and drop breakup in microchannels, vol 11

Arratia PE, Gollub JP, Durian DJ (2008) Polymeric filament thinning and breakup in microchannels, vol 77

Basaran OA (2002) Small-scale free surface flows with breakup: drop formation and emerging applications. AIChE J 48(9):1842–1848

Bazilevskii AV, Entov VM, Rozhkov AN (2001) Breakup of an oldroyd liquid bridge as a method for testing the rheological properties of polymer solutions. Polym Sci Ser A 43(7):716–726

Bazilevsky AV, Entov VM, Rozhkov AN (1990) Liquid filament microrheometer and some of its applications. In: Third European Rheology Conference and Golden Jubilee Meeting of the British Society of Rheology. Springer, pp 41–43

Bazilevsky AV, Entov VM, Rozhkov AN (2011) Breakup of a liquid bridge as a method of rheological testing of biological fluids. Fluid Dyn 46(4):613

Bhat PP, Appathurai S, Harris MT, Pasquali M, McKinley GH, Basaran OA (2010) Formation of beads-on-a-string structures during break-up of viscoelastic filaments. Nat Phys 6(8):625–631

Brandrup J, Immergut EH, Grulke EA, Abe A, Bloch DR (1989) Polymer handbook, vol 7, Wiley

Campo-Deano L, Clasen C (2010) The slow retraction method (SRM) for the determination of ultra-short relaxation times in capillary breakup extensional rheometry experiments. J Non-Newtonian Fluid Mech 165(23):1688–1699

Christanti Y, Walker LM (2001) Surface tension driven jet break up of strain-hardening polymer solutions. J Non-Newtonian Fluid Mech 100(1):9–26

Christanti Y, Walker LM (2002) Effect of fluid relaxation time of dilute polymer solutions on jet breakup due to a forced disturbance. J Rheol 46(3):733–748

Christopher GF, Anna SL (2009) Passive breakup of viscoelastic droplets and filament self-thinning at a microfluidic T-junction. J Rheol 53(3):663–683

Clasen C, Eggers J, Fontelos MA, Li J, McKinley GH (2006a) The beads-on-string structure of viscoelastic threads. J Fluid Mech 556:283–308

Clasen C, Plog JP, Kulicke W-M, Owens M, Macosko C, Scriven LE, Verani M, McKinley GH (2006b) How dilute are dilute solutions in extensional flows? J Rheol 50(6):849–881

Clasen C, Verani M, Plog JP, McKinley GH, Kulicke WM (2004) Effects of polymer concentration and molecular weight on the dynamics of visco-elasto-capillary breakup

Cogswell FN (1972) Measuring the extensional rheology of polymer melts. Trans Soc Rheol 16(3):383–403

Collier JR, Romanoschi O, Petrovan S (1998) Elongational rheology of polymer melts and solutions. J Appl Polym Sci 69(12):2357–2367

Cooper-White JJ, Fagan JE, Tirtaatmadja V, Lester DR, Boger DV (2002) Drop formation dynamics of constant low-viscosity, elastic fluids. J Non-Newtonian Fluid Mech 106(1):29–59

de Gans B-J, Duineveld PC, Schubert US (2004) Inkjet printing of polymers: state of the art and future developments. Adv Mater 16(3):203–213

De Gennes PG (1974) Coil-stretch transition of dilute flexible polymers under ultrahigh velocity gradients. J Chem Phys 60(12):5030–5042

De Menech M, Garstecki P, Jousse F, Stone HA (2008) Transition from squeezing to dripping in a microfluidic t-shaped junction. J Fluid Mech 595:141–161

Dinic J, Zhang Y, Jimenez LN, Sharma V (2015) Extensional relaxation times of dilute, aqueous polymer solutions. ACS Macro Lett 4(7):804–808

Dinic J, Jimenez LN, Sharma V (2017) Pinch-off dynamics and dripping-onto-substrate (DoS) rheometry of complex fluids. Lab Chip 17:460–473

Dylla-Spears R, Townsend JE, Jen-Jacobson L, Sohn LL, Muller SJ (2010) Single-molecule sequence detection via microfluidic planar extensional flow at a stagnation point. Lab Chip 10(12):1543–1549

Entov VM, Hinch EJ (1997) Effect of a spectrum of relaxation times on the capillary thinning of a filament of elastic liquid. J Non-Newtonian Fluid Mech 72(1):31–53

Ewoldt RH, Johnston MT, Caretta LM (2015) Experimental challenges of shear rheology: how to avoid bad data. In: Complex fluids in biological systems. Springer, pp 207–241

Feng J, Leal LG (2000) Transient extension and relaxation of a dilute polymer solution in a four-roll mill. J Non-Newtonian Fluid Mech 90(1):117–123

Flory PJ (1953) Principles of polymer chemistry. Cornell University Press, New York

Friend J, Yeo L (2010) Fabrication of microfluidic devices using polydimethylsiloxane, vol 4, Biomicrofluidics

Fuller GG, Cathey CA, Hubbard B, Zebrowski BE (1987) Extensional viscosity measurements for low-viscosity fluids. J Rheol 31(3):235–249

Galindo-Rosales FJ, Alves MA, Oliveira MSN (2013) Microdevices for extensional rheometry of low viscosity elastic liquids: a review. Microfluid Nanofluid 14(1-2):1–19

Garstecki P, Fuerstman MJ, Stone HA, Whitesides GM (2006) Formation of droplets and bubbles in a microfluidic T-junction—scaling and mechanism of break-up. Lab Chip 6(3):437–446

Graessley WW (1980) Polymer chain dimensions and the dependence of viscoelastic properties on concentration, molecular weight and solvent power. Polymer 21(3):258–262

Gyr A, Bewersdorff HW (2013) Drag reduction of turbulent flows by additives, vol 32, Springer, Berlin

Harrison GM, Boger DV (2000) Well-characterized low viscosity elastic liquids. Appl Rheol 10(4):166–177

Haward SJ (2014) Characterization of hyaluronic acid and synovial fluid in stagnation point elongational flow. Biopolymers 101(3):287–305

Haward SJ, Oliveira MSN, Alves MA, McKinley GH (2012) Optimized cross-slot flow geometry for microfluidic extensional rheometry, vol 109

Hinch EJ (1974) Mechanical models of dilute polymer solutions for strong flows with large polymer deformations. *Polymères et Lubrification*, pp 351–372

Haward SJ (2016) Microfluidic extensional rheometry using stagnation point flow, vol 10

Hoath SD, Hsiao WK, Martin GD, Jung S, Butler SA, Morrison NF, Harlen OG, Yang LS, Bain CD, Hutchings IM (2015) Oscillations of aqueous pedot Pss fluid droplets and the properties of complex fluids in drop-on-demand inkjet printing. J Non-Newtonian Fluid Mech 223:28–36

Hudson SD, Phelan FRJr, Handler MD, Cabral JT, Migler KB, Amis EJ (2004) Microfluidic analog of the four-roll mill. Appl Phys Lett 85(2):335–337

Husny J, Cooper-White JJ (2006) The effect of elasticity on drop creation in t-shaped microchannels. J Non-Newtonian Fluid Mech 137(1):121–136

James DF, Walters K (1993) A critical appraisal of available methods for the measurement of extensional properties of mobile systems. In: Techniques in rheological measurement. Springer, pp 33–53

Jones DM, Walters K (1989) The behaviour of polymer solutions in extension-dominated flows, with applications to enhanced oil recovery. Rheol Acta 28(6):482–498

Keshavarz B, Sharma V, Houze EC, Koerner MR, Moore JR, Cotts PM, Threlfall-Holmes P, McKinley GH (2015) Studying the effects of elongational properties on atomization of weakly viscoelastic solutions using Rayleigh Ohnesorge jetting extensional rheometry (ROJER). J Non-Newtonian Fluid Mech 222:171–189

Kolte MI, Szabo P (1999) Capillary thinning of polymeric filaments. J Rheol 43(3):609–625

Lee JS, Dylla-Spears R, Teclemariam NP, Muller SJ (2007) Microfluidic four-roll mill for all flow types, vol 90

Li J, Fontelos MA (2003) Drop dynamics on the beads-on-string structure for viscoelastic jets: a numerical study. Phys Fluids 15(4):922–937

Liang RF, Mackley MR (1994) Rheological characterization of the time and strain dependence for polyisobutylene solutions. J Non-Newtonian Fluid Mech 52(3):387–405

Link DR, Anna SL, Weitz DA, Stone HA (2004) Geometrically mediated breakup of drops in microfluidic devices, vol 92

Lister JR, Stone HA (1998) Capillary breakup of a viscous thread surrounded by another viscous fluid. Phys Fluids 10(11):2758–2764

Macosko CW (1994) Rheology: principles, measurements, and applications. Wiley-VCH, New Jersey

Marshall KA, Liedtke AM, Todt AH, Walker TW (2017) Extensional rheometry with a handheld mobile device. Exp Fluids 6(58):1–9

Matta JE, Tytus RP (1990) Liquid stretching using a falling cylinder. J Non-Newtonian Fluid Mech 35(2-3):215–229

Mckinley GH (2005a) Dimensionless groups for understanding free surface flows of complex fluids. Society of Rheology Bulletin 2005:6–9

Mckinley GH (2005b) Visco-elasto-capillary thinning and break-up of complex fluids. Rheology Rev 2005(3):1–48

McKinley GH, Sridhar T (2002) Filament-stretching rheometry of complex fluids. Ann Rev Fluid Mech 34(1):375–415

McKinley GH, Tripathi A (2000) How to extract the newtonian viscosity from capillary breakup measurements in a filament rheometer. J Rheol 44(3):653–670

MicroChem (n.d.) Permanent epoxy negative photoresist processing guidelines for: SU-8 2100 and SU-8 2150. https://cleanroom.byu.edu/sites/cleanroom.byu.edu/files/pdf/SU-82000DataSheet2100and2150Ver5-1.pdf

Miller E, Clasen C, Rothstein JP (2009) The effect of step-stretch parameters on capillary breakup extensional rheology (CaBER) measurements. Rheol Acta 48(6):625–639

Morrison NF, Harlen OG (2010) Viscoelasticity in inkjet printing. Rheol Acta 49(6):619–632

Nguyen DA, Gupta RK, Sridhar T (1990) Experimental results and constitutive modeling of the extensional flow of M1. J Non-Newtonian Fluid Mech 35(2):207–214

Oliveira MSN, McKinley GH (2005) Iterated stretching and multiple beads-on-a-string phenomena in dilute solutions of highly extensible flexible polymers, vol 17

Oliveira MSN, Yeh R, McKinley GH (2006) Iterated stretching, extensional rheology and formation of beads-on-a-string structures in polymer solutions. J Non-Newtonian Fluid Mech 137(1):137–148

Öttinger HC (2012) Stochastic processes in polymeric fluids: tools and examples for developing simulation algorithms. Springer Science & Business Media

Paterson RW, Abernathy FH (1970) Turbulent flow drag reduction and degradation with dilute polymer solutions. J Fluid Mech 43(4):689–710

Petrie CJS (2006) Extensional viscosity: a critical discussion. J Non-Newtonian Fluid Mech 137(1):15–23

Renardy M (1995) A numerical study of the asymptotic evolution and breakup of Newtonian and viscoelastic jets. J Non-Newtonian Fluid Mech 59(2-3):267–282

Rodd LE, Scott TP, Cooper-White JJ, McKinley GH (2005) Capillary break-up rheometry of low-viscosity elastic fluids. Appl Rheol 15(1):12–27

Savins JG (1964) Drag reduction characteristics of solutions of macromolecules in turbulent pipe flow. Soc Pet Eng J 4(03):203–214

Schümmer P, Tebel KH (1983) A new elongational rheometer for polymer solutions. J Non-Newtonian Fluid Mech 12(3):331–347

Schummer P, Tebel KH (1982) Production of monodispersed drops by forced disturbance of a free jet. German Chemical Engineering 5:209–220

Sharma V, Haward SJ, Serdy J, Keshavarz B, Soderlund A, Threlfall-Holmes P, McKinley GH (2015) The rheology of aqueous solutions of ethyl hydroxy-ethyl cellulose (EHEC) and its hydrophobically modified analogue (hmEHEC): extensional flow response in capillary break-up, jetting (ROJER) and in a cross-slot extensional rheometer. Soft Matter 11(16):3251–3270

Sousa PC, Vega EJ, Sousa RG, Montanero JM, Alves MA (2017) Measurement of relaxation times in extensional flow of weakly viscoelastic polymer solutions. Rheol Acta 56(1):11–20

Spiegelberg SH, Ables DC, McKinley GH (1996) The role of end-effects on measurements of extensional viscosity in filament stretching rheometers. J Non-Newtonian Fluid Mech 64(2):229–267

Stelter M, Brenn G, Yarin AL, Singh RP, Durst F (2000) Validation and application of a novel elongational device for polymer solutions. J Rheol 44(3):595–616

Stone HA (1994) Dynamics of drop deformation and breakup in viscous fluids. Ann Rev Fluid Mech 26(1):65–102

Stone HA, Leal LG (1989) Relaxation and breakup of an initially extended drop in an otherwise quiescent fluid. J Fluid Mech 198:399–427

Stone HA, Leal GL (1990) The effects of surfactants on drop deformation and breakup. J Fluid Mech 220:161–186

Stone HA, Bentley BJ, Leal LG (1986) An experimental study of transient effects in the breakup of viscous drops. J Fluid Mech 173:131–158

Teraoka I (2002) Models of polymer chains. Wiley, New Jersey

Tirtaatmadja V, McKinley GH, Cooper-White JJ (2006) Drop formation and breakup of low viscosity elastic fluids: effects of molecular weight and concentration, vol 18

Tjahjadi M, Stone HA, Ottino JM (1992) Satellite and subsatellite formation in capillary breakup. J Fluid Mech 243:297–317

Tuladhar TR, Mackley MR (2008) Filament stretching rheometry and break-up behaviour of low viscosity polymer solutions and inkjet fluids. J Non-Newtonian Fluid Mech 148(1):97–108

van Steijn V, Kleijn CR, Kreutzer MT (2010) Predictive model for the size of bubbles and droplets created in microfluidic T-junctions. Lab Chip 10(19):2513–2518

Virk PS (1975) Drag reduction fundamentals. AIChE J 21(4):625–656

Wagner C, Bourouiba L, McKinley GH (2015) An analytic solution for capillary thinning and breakup of fene-p fluids. J Non-Newtonian Fluid Mech 218:53–61

Wagner C, Amarouchene Y, Bonn D, Eggers J (2005) Droplet detachment and satellite bead formation in viscoelastic fluids, vol 95

Walker TW, Hsu TT, Fitzgibbon S, Frank CW, Mui DSL, Ji Z, Mendiratta A, Fuller GG (2014) Enhanced particle removal using viscoelastic fluids. J Rheol 58(1):63–88

Wever DAZ, Picchioni F, Broekhuis AA (2011) Polymers for enhanced oil recovery: a paradigm for structure–property relationship in aqueous solution. Prog Polym Sci 36(11):1558–1628

Xu D, Sanchez-Romaguera V, Barbosa S, Travis W, de Wit J, Swan P, Yeates SG (2007) Inkjet printing of polymer solutions and the role of chain entanglement. J Mater Chem 17(46):4902–4907

Xu JH, Li SW, Tan J, Wang YJ, Luo GS (2006) Preparation of highly monodisperse droplet in a T-junction microfluidic device. AIChE J 52(9):3005–3010

Xu JH, Li SW, Tan J, Luo GS (2008) Correlations of droplet formation in T-junction microfluidic devices: from squeezing to dripping. Microfluid Nanofluid 5(6):711–717

Yarin AL (1993) Free liquid jets and films: hydrodynamics and rheology. Longman Publishing Group, Harlow

Zhong L, Oostrom M, Truex MJ, Vermeul VR, Szecsody JE (2013) Rheological behavior of xanthan gum solution related to shear thinning fluid delivery for subsurface remediation. J Hazard Mater 244:160–170